

Entangled qutrits for quantum communication

R. T. Thew,* A. Acín,[†] H. Zbinden, and N. Gisin

Group of Applied Physics, University of Geneva, 1211 Geneva 4, Switzerland

(Dated: May 6, 2019)

We introduce a new technique to experimentally generate, control and measure entangled qutrits, 3-dimensional quantum systems. This scheme uses spontaneous parametric down converted photons and unbalanced 3-arm fiber optic interferometers in a scheme analogous to the Franson interferometric arrangement for qubits. The results reveal a source capable of generating maximally entangled states with a net state fidelity, $F = 0.985 \pm 0.018$. Further the control over the system reveals a high, net, 2-photon interference fringe visibility, $V = 0.919 \pm 0.026$, when the two phases are varied. This has all been done at telecom wavelengths thus facilitating the advancement to long distance higher dimensional quantum communication.

PACS numbers: 03.67.Hk, 03.67.Lx

Quantum information science is now a well recognized branch of science in its own right, dealing with a diverse range of theoretical and practical issues related to quantum computing and quantum communication [1]. It exists today because we, as a community of physicists, computer scientists and others, chose to think differently. We took a positive approach to what had been the paradoxical aspects of quantum physics. From this we have gained in our understanding of fundamental physics with the added bonus of finding practical applications for quantum systems. Already we have quantum key distribution [2] as the first quantum technology to be taken into the public domain. At the heart of this revolution has been the idea of the Qubit, simply, a two dimensional quantum system. The question that has received significant theoretical interest in the last few years is - what can we do with higher dimensional systems?

There has recently been several proposals for quantum communication protocols involving higher dimensional states, specifically qutrits (three dimensional quantum systems). In some cases these have advantages over qubit protocols, like increased robustness against noise in quantum key distribution schemes [12, 13, 14]. However, the more interesting cases are those where it is more efficient to have a system encoded using qutrits than qubits, like for the solution to the Byzantine Agreement Problem [16] or for Quantum Coin Tossing [18]. As such we want an efficient source of entangled qutrits to take advantage of these protocols. Also with respect to our opening remarks, if we can approach these qutrit and higher dimensional systems with a positive perspective then what we have is a larger quantum system in which to perform even more complex quantum protocols.

There are two possible approaches that can be taken if we want to investigate higher dimensional systems: use multiple (more than 2) entangled qubit systems [3, 4, 5, 6, 7]; or increase the dimensions of the fundamental elements. If we increase the dimensions of the elements, the simplest place to start to answer some of

the questions experimentally is with qutrits. Recently there have been some advances to this end: the generation of qutrits using bi-photons [8]; and two schemes generating entangled qudits, d -level quantum systems. The first, using the orbital angular momentum of light, have specifically shown their scheme setup to analyze qutrits [9], while the second uses a pulsed, mode-locked, laser to generate time-bin qudits where they have shown entanglement up to $d = 11$ [10].

In this Letter we introduce an experimental setup where we can generate, manipulate and measure entangled qutrits. The scheme we use is based on energy-time entanglement and is analogous to the Franson-type interferometric arrangement for photonic qubits [11]. We first detail our experimental set-up and show how this corresponds to the theoretical description of qutrits before deriving two different means of analyzing the output of the system.

Consider the experimental schematic of Fig.1. We have a CW laser at 657 nm incident on a Periodically Poled Lithium Niobate (PPLN) waveguide where spontaneous Parametric Down Conversion (PDC) produces degenerate, collinear, energy-time entangled photon pairs at 1314 nm [15]. The photon pairs are coupled into a monomode optical fiber before passing through a fiber beam splitter (BS) which separates the photons and sends them to one of the two all-fiber Michelson interferometers. The interferometers each have three arms of different length such that the path-length difference in both interferometers are the same, within the coherence length of the PDC photons. When the photons enter the interferometers via the 6-port symmetric couplers [19] T_A and T_B , also known as Tritters, they have a choice of three paths, thus generating our qutrit space. We encode these paths via the path-lengths, ie. short, medium, long, or 0,1,2, as labelled. At the ends of these arms we use Faraday Mirrors so that when a photon returns to the tritter its polarization is orthogonal to when they entered, *regardless of the path taken*, thus reducing the

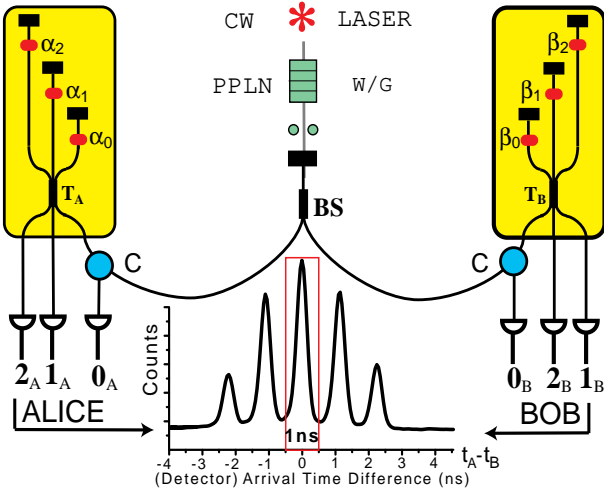


FIG. 1: Schematic of experiment for generation and analysis of entangled qutrits: Down-Converted photon pairs at telecom wavelengths combined with unbalanced three path interferometers are used to generate and analyze energy-time entangled qutrits.

which-path information which would reduce their indistinguishability and hence diminish the quality of the entanglement resource.

When the photons leave the interferometers there are nine possible coincidence detection combinations that we can observe between each of Alice and Bob's three detectors. We can put optical Circulators (C) on one input port of each interferometer so we can detect all of these. A coincidence detection between Alice and Bob can only take place under the following circumstances: The two photons took the same path in their respective interferometers, ie. both short, both medium or both long; The coherence length of the PDC photons is much smaller than the path-length difference ($40 \text{ nm} \ll 24 \text{ cm}$) so that no single photon interference effects are observed; The coherence length of the pump laser (Toptica DL100) is much greater than these path-length differences ($48 \text{ cm} \ll \mathcal{O}(100 \text{ m})$) so that we have no timing information as to the creation time of the photon pair and hence which path was taken before the coincidence measurement.

We use symmetric trititers and equalize the losses in the three arms as much as possible to simplify both the theory and experiment. With this symmetry we find that instead of nine detection possibilities we can observe just three knowing that the others should be equivalent to these. More specifically, we can consider the various post-selected states, those that lead to a coincidence detection at the different outputs for Alice and Bob,

$$|\psi_{00}\rangle = \frac{1}{\sqrt{27}}[|00\rangle + e^{i(\alpha_1 - \alpha_0 + \beta_1 - \beta_0 + t)}|11\rangle + e^{i(\alpha_2 - \alpha_0 + \beta_2 - \beta_0 + t)}|22\rangle] \quad (1)$$

$$|\psi_{01}\rangle = \frac{1}{\sqrt{27}}[|00\rangle + e^{i(\alpha_1 - \alpha_0 + \beta_1 - \beta_0)}|11\rangle + e^{i(\alpha_2 - \alpha_0 + \beta_2 - \beta_0 - t)}|22\rangle] \quad (2)$$

$$|\psi_{02}\rangle = \frac{1}{\sqrt{27}}[|00\rangle + e^{i(\alpha_1 - \alpha_0 + \beta_1 - \beta_0 - t)}|11\rangle + e^{i(\alpha_2 - \alpha_0 + \beta_2 - \beta_1)}|22\rangle]. \quad (3)$$

Here $|\psi_{01}\rangle$ denotes the state post-selected by detection at Alice's detector 0 and Bob's detector 1. $|11\rangle = |1\rangle_A \otimes |1\rangle_B$ corresponds to the photon taking the medium path in both interferometers. We have also introduced the factor $t = 2\pi/3$ which is the phase obtained changing ports in the trititers, analogous to the $\pi/2$ phase obtained upon reflection in normal 4-port beam-splitters. The previously mentioned symmetry ensures that the states satisfy, $|\psi_{00}\rangle = |\psi_{11}\rangle = |\psi_{22}\rangle$, $|\psi_{01}\rangle = |\psi_{12}\rangle = |\psi_{20}\rangle$, and $|\psi_{02}\rangle = |\psi_{10}\rangle = |\psi_{21}\rangle$.

For detection we are using a combination of Ge and InGaAs Avalanche Photo-Diodes (APDs). The Ge work in a passive mode at 1314 nm and have efficiencies, $\eta_{Ge} \approx 10\%$. We use these on one side, Alice's, to trigger the InGaAs detectors (idQuantique id200) on Bob's side which need to be used in a gated mode but have a higher quantum efficiency, $\eta_{InGaAs} > 20\%$, and better noise characteristics. We use a Time-To-Digital converter to process these detection events and generate data corresponding to arrival time differences between the start (Alice) and the three different stops (Bob). For each of these start-stop combinations we obtain an histogram like the one inset between Alice and Bob's detectors in Fig.1. Only the fit to the experimental histogram is shown for clarity. We see five prominent peaks which correspond to the different possible arrival times, due to which path is taken, between the photons arriving at Alice's and Bob's. The central peak corresponds to $\Delta t = 0$, ie. photons arriving at the same time. We can select all events occurring within some temporal window $\Delta\tau_w = 1 \text{ ns}$ about this peak which corresponds to a projection onto one of the states previously listed.

The other peaks here are not without interest. The first two lateral peaks project onto different subspaces within the entangled qutrit Hilbert space. Specifically, detecting events in these peaks projects onto states of the form,

$$|\psi_{00}^R\rangle = \frac{1}{\sqrt{27}}[|01\rangle + e^{i(\alpha_1 - \alpha_0 + \beta_2 - \beta_1 - t)}|12\rangle] \quad (4)$$

for the right peak. This state corresponds to where the photons arrive with a fixed time difference, $\Delta\tau = 1.2 \text{ ns}$, due to the path-length differences. But there are two possibilities and we cannot distinguish photons that took the short path at Alice's and the medium path at Bob's from those that took the medium at Alice's and the long at Bob's. The left peak corresponds to those states having an arrival time difference of $-\Delta\tau$, the left peak, and

these project onto states of the form

$$|\psi_{00}^L\rangle = \frac{1}{\sqrt{27}}[|10\rangle + e^{i(\alpha_2 - \alpha_1 + \beta_1 - \beta_0 - t)}|21\rangle] \quad (5)$$

with the opposite path relationships. Both left and right states here are entangled and their form is suggestive of the type of states required for optimal quantum coin tossing protocol [18]. We have the same symmetry for the other detectors, as previously shown for the states in the central peak, and again these results differ by factors of t . The outer two peaks correspond to two time-bins, $\pm 2\Delta\tau$, difference in arrival times, ie. $|02\rangle$ and $|20\rangle$, with no interfering effects present.

We commented that states corresponding to these lateral peaks were interesting but they are also useful in controlling and characterizing the entangled qutrits of the central peak. We will vary the phases in just one, Alice's, interferometer, thus we can think of Bob's interferometer as a reference and set all of these phases settings to zero, $(\beta_0, \beta_1, \beta_2) = (0, 0, 0)$. If we do this we find that the lateral peaks now have corresponding states of the form:

$$\begin{aligned} |\psi_{00}^R\rangle &= |01\rangle + e^{i(\Phi_{00}^R + t)}|12\rangle : \Phi_{00}^R \equiv \alpha_1 - \alpha_0 + t \\ |\psi_{00}^L\rangle &= |10\rangle + e^{i(\Phi_{00}^L - t)}|21\rangle : \Phi_{00}^L \equiv \alpha_2 - \alpha_1, \end{aligned} \quad (6)$$

and similarly for the others, although the three are phase shifted by the factor t with respect to one another. We can then rewrite the entangled qutrit states of Eq.(1) as

$$|\psi_{00}\rangle = \frac{1}{\sqrt{27}}[|00\rangle + e^{i\Phi_{00}^R}|11\rangle + e^{i(\Phi_{00}^R + \Phi_{00}^L)}|22\rangle]. \quad (7)$$

In fact all three different states can be written in this form with the phase shift of t within the definition of the phase of the lateral peaks. Thus, if we are trying to align the interferometers or determine some relative phases we can observe the various probabilities of coincidence in the associated peak of the time-of-arrival histogram to assist us. By observing the behavior of these three peaks we can control the relationship between the two phases. We control the phase, its setting and stability, via temperature. As the fiber is heated it gets longer and thus the phase relative to the other fiber arms is shifted. This is done such that there is a fixed relationship between the two phases, like $\Phi_{jk}^R = r\Phi_{jk}^L$, where r is a constant coefficient.

So how can we characterize and quantify these states? From the perspective of the optician we would like to be able to define some interference fringe visibility to quantify the process. This can always be defined as $V = (I_{max} - I_{min})/(I_{max} + I_{min})$ where, in the case of single photon detection, we can replace these maximum and minimum intensities with detection probabilities, with the limits taken over all possible phases.

Before we determine the detection probabilities for these qutrit states we have defined we will introduce a

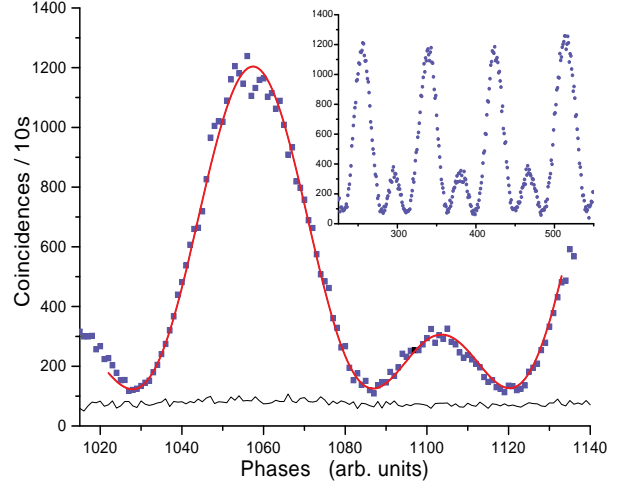


FIG. 2: Raw interference fringe, coincidence counts, for the central peak. The accidental coincidence (noise) level is also shown. Inset we see another interference pattern showing the stability and repeatability of the source.

standard, symmetric, noise model such that we can consider the case where we have,

$$\rho_{jk} = \lambda|\psi_{jk}\rangle\langle\psi_{jk}| + \frac{1-\lambda}{9}I_9. \quad (8)$$

With probability λ we expect our entangled qutrit state, and with probability $(1-\lambda)$ we expect a maximally mixed state, at output jk . If we do this we have the following probability for a coincidence detection projecting onto the mixed state of Eq.(8),

$$P_{jk} = \frac{1}{27} [3 + 2\lambda [\cos(\Phi_{jk}^R) + \cos(\Phi_{jk}^L) + \cos(\Phi_{jk}^R + \Phi_{jk}^L)]] . \quad (9)$$

We can clearly see the dependence of the phases associated with the right and left lateral peaks, as well as the sum of their values. From this we can derive quantities such as the fidelity and visibility. The fidelity is defined, with respect to a maximally entangled qutrit state, as $F = \text{Tr}[\rho\psi_{me}] = (1 + 8\lambda)/9$.

It is clear from the form of Eq.(8) that the interference fringes resulting from varying the two phases will be qualitatively and quantitatively different from those of qubits which depend on just one sinusoidal function. One result of this is that we no longer have a simple relationship between fidelity and visibility that qubits provide. To obtain a qualitative relationship between these in the qutrit regime we need to satisfy very specific constraints for the two phases. The simplest relationship demands that we maintain the constant relationship, $\Phi_{jk}^R = \Phi_{jk}^L$, as we scan the two phases.

In Fig.2 we see the coincidence count rate as the phases are scanned in this manner. The points are the experimental results and the solid line is a least-squares fit based on the function given in Eq.(9). In doing this the

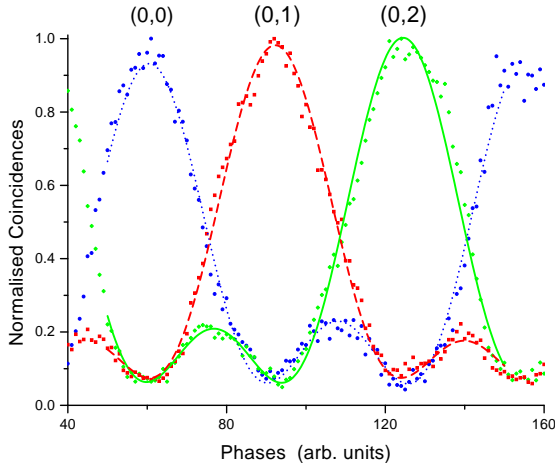


FIG. 3: Normalized interference fringes, as in Fig.2, for the three possible coincidence detections highlighting the three-fold symmetry.

fit is parameterized by λ and we can determine the fidelity of our source using the definition previously stated. Indirectly we can also use this fit to find the maximum and minimum and hence also the visibility. The results for both the net (noise subtracted) and raw Fidelity are $F_{net} = 0.984 \pm 0.018$ and $F_{raw} = 0.843 \pm 0.016$. The noise consists of accidental coincidences due to detector noise and uncorrelated photons and is measured concurrently with the true coincidence counts. The noise level is shown just below the raw interference fringe in Fig.2. We also find visibilities of $V_{net} = 0.919 \pm 0.026$ and $V_{raw} = 0.815 \pm 0.021$. In the inset we have also shown a longer section of data illustrating the control and stability of this source.

In Fig.3 we see the normalized (accounting for variation in detection efficiency) coincidences and fits for all three coincidence outcomes measured at the same time. These all have the same form as that of Fig.2 but are equally distributed with respect to the phase axis. This separation corresponds to the $t = 2\pi/3$ phase shift between the three possible outcomes. While we clearly see the 3-fold symmetry we also see that it is not perfect. The alignment between the minima and maxima changes slightly from one period to the next. This is, in part, because ratio between the two phases, r , is not exactly one and this variation in turn reduces the visibility. This is why, although we have very high fidelity, the visibility is not closer to one. Indeed if we were to consider performing

a Bell test, like that proposed by Collins *et al.* [17], it would suggest that our source is capable of violating this by more than 14σ (the critical fidelity for violating the Bell inequality can be shown to be $F_c=0.726$). However, the constraints on the relationship between the two phases are stricter than what we have considered here.

We have presented a scheme to generate, control and measure entangled qutrits. This is done at telecom wavelengths where entanglement of this kind has already been shown to be robust and an ideal resource for long distance quantum communication in the qubit regime [20]. The results show a resource capable of producing high fidelity maximally entangled qutrits with good controllability for quantum communication.

The Authors would like to acknowledge useful discussions with S. P. Kulik and his group through INTAS and the technical assistance of J-D.Gautier. This project is financed by the Swiss NCCR "Quantum Photonics" and the EU IST-FET project RamboQ.

* Electronic address: Robert.Thew@physics.unige.ch

† Presently at: Institut de Ciències Fotòniques, Jordi Girona 29, 08034 Barcelona, Spain

- [1] For instance, M. A. Nielsen and I. L. Chuang, *Quantum Computation and Quantum Information*, Cambridge University Press, Cambridge, (2001).
- [2] N. Gisin *et al.*, Rev. Mod. Phys., **74**, 145 (2002).
- [3] C. A. Sackett *et al.*, Nature **404**, 256 (2000).
- [4] J. Pan *et al.*, Nature (London) **403**, 515 (2000).
- [5] T. Jennewein *et al.*, Phys. Rev. Lett. **88**, 017903 (2002).
- [6] J. C. Howell, *et al.*, Phys. Rev. Lett. **88**, 030401 (2002).
- [7] I. Marcikic *et al.*, Nature, **421**, 509 (2003).
- [8] A. V. Burlakov *et al.*, quant-ph/0207096 (2002).
- [9] A. Vaziri, G. Weihs, and A. Zeilinger, Phys. Rev. Lett. **89**, 240401 (2002).
- [10] H. de Riedmatten, I. Marcikic, H. Zbinden and N. Gisin, Quant. Inf. and Comp., **2** 6, 425 (2002).
- [11] J. D. Franson, Phys. Rev. Lett. **62**, 2205 (1989).
- [12] H. Bechmann-Pasquinucci and A. Peres, Phys. Rev. Lett. **85**, 3313 (2000).
- [13] N. J. Cerf *et al.*, Phys. Rev. Lett. **88**, 127902 (2002).
- [14] D. Bru β and C. Macchiavello, Phys. Rev. Lett. **88**, 127901 (2002).
- [15] S. Tanzilli *et al.*, Elect. Lett., **37**, 28 (2001).
- [16] M. Fitzi *et al.*, Phys. Rev. Lett., **87** 217901 (2001).
- [17] D. Collins *et al.*, Phys. Rev. Lett., **88**, 040404 (2002).
- [18] A. Ambainis, Proc. STOC 01, 134 (2001).
- [19] M. Zukowski *et al.*, Phys. Rev. A **55**, 2564 (1997).
- [20] R. T. Thew *et al.*, Phys. Rev. A **66**, 062304 (2002).